

Atmospheric correction for the KNMI Cloud Physical Properties retrieval algorithm

*Jan Fokke Meirink, Rob Roebeling
and Piet Stammes*

KNMI technical report = technisch rapport; TR-304

De Bilt, 2009

PO Box 201
3730 AE De Bilt
Wilhelminalaan 10
De Bilt
The Netherlands
<http://www.knmi.nl>
Telephone +31(0)30-220 69 11
Telefax +31(0)30-221 04 07

Authors: Meirink, J.F.
Roebeling, R.
Stammes, P.



Atmospheric correction for the KNMI Cloud Physical Properties retrieval algorithm

Jan Fokke Meirink¹, Rob Roebeling¹, and Piet Stammes¹

¹Royal Netherlands Meteorological Institute

February 17, 2009

Contents

1	Introduction	4
2	Method	4
3	Assessment of atmospheric correction factors	7
3.1	0.6 μm	7
3.2	0.8 μm	7
3.3	1.6 μm	7
3.4	2.1 μm	11
3.5	3.8 μm	11
4	Impact on CPP retrievals	11
5	Future work and improvements	14
6	Summary	15
A	MODTRAN input file	15
B	Spectral Response Funtions	15
C	List of acronyms	16

Abstract

A procedure is described to correct monochromatic reflectances simulated by a radiative transfer model to narrow-band reflectances measured by a satellite imager and affected by trace-gas absorption in the atmosphere. This atmospheric correction scheme has been implemented in the KNMI/CM-SAF Cloud Physical Properties (CPP) retrieval algorithm, version 3.0. Correction factors have been calculated for three satellite instruments (SEVIRI, MODIS, and AVHRR) and five spectral bands (around wavelengths 0.6, 0.8, 1.6, 2.1, and 3.8 μm). The effect of atmospheric correction on CPP retrievals based on the 0.6- and 1.6- μm bands is illustrated using SEVIRI data over Europe. On average, the cloud optical thickness increases by $\sim 3\%$, while the particle effective radius decreases by $\sim 10\%$.

1 Introduction

Cloud physical properties are commonly retrieved from satellite imagers using a method described by Nakajima and King (1990). This method is based on the fact that cloud-reflected solar radiation at non-absorbing (by liquid water and ice crystals) wavelengths, like $0.6 \mu\text{m}$, is dominated by the cloud optical thickness τ , while the reflectance at absorbing wavelengths, like $1.6 \mu\text{m}$, is mainly a function of the effective radius r_e of cloud droplets or ice crystals. Retrievals are generally performed by comparing observed reflectances to reflectances simulated with a radiative transfer model (RTM) and stored in lookup tables for a range of viewing geometries, cloud optical thicknesses and effective radii. Normally, the RTM simulations do not take into account the absorption of radiation by trace gases in the atmosphere. The procedure to account for the effect of absorption is called atmospheric correction (e.g., Vermote et al. 1997).

In this report the development of an atmospheric correction procedure is presented for the KNMI Cloud Physical Properties (CPP) retrieval algorithm (Roebeling et al. 2006), developed in the framework of EUMETSAT's Satellite Application Facility on Climate Monitoring (CM-SAF, Schulz et al. 2008). Following up on a study by Podlasly (2002), which focused on characterizing the relation between surface and top-of-atmosphere (TOA) reflectivity, we use MODTRAN (Berk et al. 1989; 2000) to assess the impact of absorption by atmospheric trace gases on band-averaged reflectances as observed by satellite instruments. Three instruments are considered: SEVIRI on MSG, MODIS on the EOS satellites Terra and Aqua, and AVHRR on the NOAA and METOP satellites. The atmospheric correction is not only assessed for the $0.6\text{-}\mu\text{m}$ and $1.6\text{-}\mu\text{m}$ channels, which are used as non-absorbing and absorbing wavelength bands in CPP at the moment, but also for the $0.8\text{-}\mu\text{m}$ channel, which the MODIS group uses as alternative non-absorbing band over ocean, the $2.1\text{-}\mu\text{m}$ channel, which the MODIS group uses as absorbing channel, and the $3.8\text{-}\mu\text{m}$ channel, for which the CPP algorithm will be adapted to allow retrievals from AVHRR back to the first NOAA satellites.

In Section 2 the applied methodology will be outlined. Section 3 illustrates the magnitude of the atmospheric correction for the different wavelength bands. The impact on CPP retrievals is assessed in Section 4. Plans for future improvements to the atmospheric correction procedure are outlined in Section 5, and a summary of the results is given in Section 6.

2 Method

The monochromatic atmospheric reflectance R_λ at wavelength λ – as observed from space – can be written as follows (e.g., Liou 2002):

$$R_\lambda = \frac{\pi I_r(\lambda)}{\mu_0 F_0(\lambda)}, \quad (1)$$

where I_r is the outgoing reflected solar radiation at TOA in the direction of the satellite in $\text{W m}^{-2} \text{sr}^{-1} \text{nm}^{-1}$, F_0 is the incoming TOA solar irradiance in $\text{W m}^{-2} \text{nm}^{-1}$, and μ_0 is the cosine of the solar zenith angle θ_0 . R_λ is a function of the viewing geometry (including the solar zenith angle, the satellite viewing zenith angle θ , and the relative sun-satellite azimuth angle ϕ), the atmospheric composition (including clouds, aerosols and gases) and the surface reflectance.

Satellite instruments measure a band-averaged reflectance \bar{R} , which is defined as follows:

$$\bar{R} = \frac{\pi I_r}{\mu_0 F_0} = \frac{\pi \int_{\lambda_1}^{\lambda_2} f(\lambda) I_r(\lambda) d\lambda}{\mu_0 \int_{\lambda_1}^{\lambda_2} f(\lambda) F_0(\lambda) d\lambda}, \quad (2)$$

where λ_1 and λ_2 are the minimum and maximum wavelengths of the band, respectively, and $f(\lambda)$ is the spectral response function (SRF) of the satellite instrument.

The CPP algorithm is based on a lookup table (LUT) of $R_{\lambda_c}^{\text{DAK}}$, the reflectance at central wavelengths of the wavelength bands observed from satellite, simulated by the radiative transfer model DAK (Stammes 2001) as a function of the viewing geometry and two key cloud physical properties: the cloud droplet effective radius r_e and the cloud optical thickness τ . In the DAK simulations, surface reflectance, Rayleigh scattering, absorption and scattering by cloud droplets, and absorption by ozone (based on a mid-latitude-summer (MLS) ozone profile) have been taken into account, but the effects of scattering and absorption by aerosols and absorption by other atmospheric gases (e.g., H_2O , CO_2 , and CH_4) have been neglected. In this study a correction method for the latter effect is developed.

We use MODTRAN4 Version 2 (Berk et al. 2000) to simulate the spectral reflectance over satellite instrument wavelength bands, for a clear sky (see next paragraph) and including Rayleigh scattering and absorption by atmospheric gases. For each choice of parameters (Table 1) two MODTRAN simulations, both with Rayleigh scattering, are performed:

1. a simulation including all atmospheric gases to provide the band-averaged reflectance \bar{R}^{MOD} , calculated using Equation 2;
2. a simulation including only ozone to provide the reflectance at the central wavelength $R_{\lambda_c}^{\text{MOD}}$, mimicing the DAK calculations.

An atmospheric correction factor c is then defined by

$$c = \frac{\bar{R}^{\text{MOD}}}{R_{\lambda_c}^{\text{MOD}}}, \quad (3)$$

and the final simulated reflectance \bar{R}^{sim} , to be compared with the observed reflectance in CPP, is:

$$\bar{R}^{\text{sim}} = cR_{\lambda_c}^{\text{DAK}}. \quad (4)$$

As a simplification and to avoid problems related to the modelling of clouds in MODTRAN (Roebeling et al. 2005), clouds are not explicitly taken into account in the MODTRAN simulations. Instead, they are represented by a Lambertian surface at the cloud top height (CTH). Hence, in- and below-cloud scattering and absorption are not taken into account for the calculation of the atmospheric correction factors. The consequences of this are discussed in Section 5). For the Lambertian surface an albedo $A_s = 0.35$ is used at all wavelengths, corresponding to a typical cloud albedo. It turns out that the actual value of A_s has a modest impact on the calculated atmospheric correction factors in the 0.6- μm channel because the Rayleigh scattering contribution to the total reflectance depends on the surface albedo. In the most extreme circumstances (extreme values of the parameters in Table 1), the difference in c resulting from a decrease of A_s to 0.15 or an increase to 0.8 is up to 2%. Under more ‘normal’ conditions, the difference is typically $\sim 0.2\%$. In the other channels, Rayleigh scattering plays hardly any role, and the atmospheric correction factor shows a negligible dependence on the chosen surface albedo.

Obviously, CTH is one of the parameters determining the atmospheric correction factor. Other such parameters are related to the viewing geometry and the concentration profiles of atmospheric gases.

Regarding the viewing geometry, it should be realized that the amount of gaseous absorption depends on the length of the light path through the atmosphere only. This length is proportional to the geometrical air-mass factor (AMF), defined as:

$$\text{AMF} = \frac{1}{\cos \theta_0} + \frac{1}{\cos \theta}. \quad (5)$$

In the MODTRAN simulations, $\theta_0 = \theta = \arccos(2/\text{AMF})$ and $\phi = 0$ are used, but – as noted above – the specific choice of the angles has a negligible influence on the calculated atmospheric correction factor.

Table 1: Settings in the MODTRAN simulations of TOA reflectance. More details can be found in the sample MODTRAN input file in Appendix A.

CTH (= surface height)	0, 1, 2, . . . , 10, 12, 14, 16, 20 km
AMF	2, 2.5, 3, . . . , 8
TCWV	0, 10, 20, . . . , 150 kg m ⁻²
CO ₂ mixing ratio	385 ppm
CH ₄ mixing ratio	1700 ppb
N ₂ O mixing ratio	320 ppb
O ₃ column	332 DU (= MLS)
water vapour profile shape	MLS
surface reflectance	0.35
spectral resolution	1 nm (5 nm for 3.8- μ m channel)

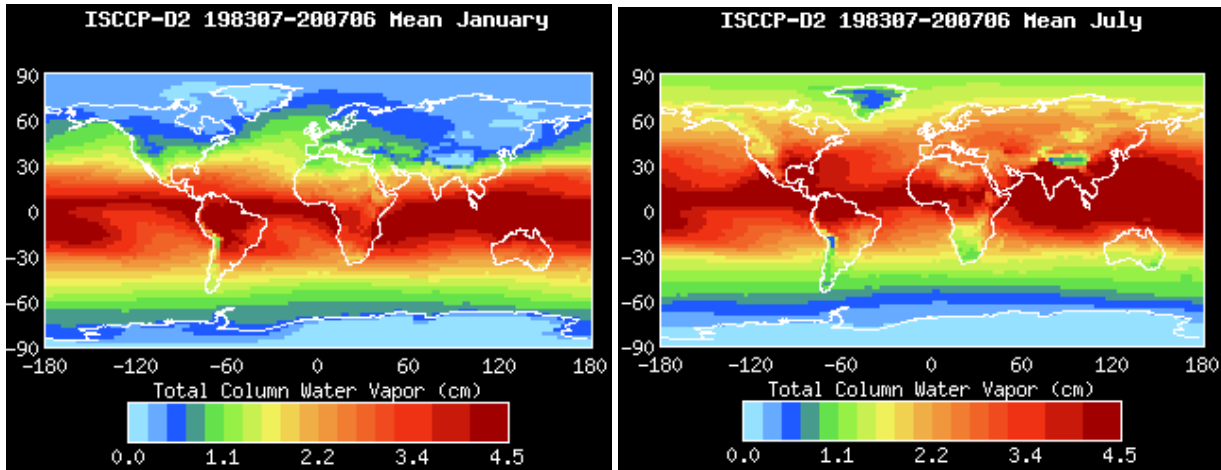


Figure 1: Climatological monthly mean TCWV for January (left) and July (right) according to ISCCP. The figures have been taken from <http://isccp.giss.nasa.gov>. 1 cm corresponds to 10 kg m⁻².

Regarding gaseous absorption, it is important to note that most absorbing gases are long-lived and therefore well-mixed in the atmosphere (see Table 1 for assumed mixing ratios). There are two exceptions: ozone and water vapour. Variations in total ozone columns are on the order of $\pm 30\%$ compared to the MLS climatological value, which translates to a similar impact on the ‘ozone part’ of the atmospheric correction factors in the 0.6- μ m channel (in other channels O₃ does not absorb). This was considered small enough to be neglected. Furthermore, since most of the ozone is in the stratosphere – thus above the clouds – variations in the vertical ozone profile shape can also be neglected.

In contrast, water vapour is highly variable (see Figure 1) and resides mostly in the lower troposphere. We decided to only consider the total column water vapour (TCWV) as a parameter in the MODTRAN simulations. In contrast, the vertical profile shape was fixed at the shape of the MLS water vapour profile. This was mainly done to limit the amount of parameters, and because information on vertical water vapour profiles is currently not available to the CPP algorithm.

Summarizing, three parameters determine the atmospheric correction factor: CTH, AMF, and TCWV. These parameters were varied over the ranges presented in Table 1. In this way, a (second) lookup table was generated, which was included in the CPP algorithm providing a correction to the DAK-simulated monochro-

matic reflectances, according to Equation (4). Within CPP an estimate of CTH is available (Roebeling and Holleman 2008), while TCWV is taken from the International Satellite Cloud Climatology Project (ISCCP) monthly climatology at a spatial resolution of $2.5^\circ \times 2.5^\circ$. Figure 1 shows two months of this dataset.

3 Assessment of atmospheric correction factors

In this section, the magnitude of atmospheric correction is assessed for five channels present on three satellite instruments: SEVIRI, MODIS, and AVHRR (see Table 2). Figure 2 shows reflectance spectra and spectral response functions ($f(\lambda)$ in Equation (2)) for the satellite instruments considered. In Table 3 the absorbing gases for the different channels are identified, and the atmospheric correction for individual gases is calculated. Figure 3 shows how the atmospheric correction depends on the parameters AMF, CTH, and TCWV. Results are presented for and with respect to a reference atmosphere, defined by the parameter settings $CTH = 2$ km, $AMF = 2$, and $TCWV = 30$ kg m⁻². The atmospheric correction factors are expressed as a percentage reduction of reflectance due to absorption, i.e.: $(1 - c) \times 100\%$.

3.1 0.6 μ m

The reflectance spectrum around 0.6 μ m (Figure 2) shows a broad O₃ absorption feature ranging from below 560 nm to about 680 nm. Additionally, absorption features by H₂O and O₂ are visible. The SRFs of SEVIRI, MODIS and AVHRR are relatively similar, with MODIS having the narrowest SRF.

Since absorption leads to a reduction in reflectance, the atmospheric correction factors expressed as a percentage reduction in reflectance should always be positive. The negative value for the effect of O₃ absorption on MODIS (see Table 3) is due to the fact that O₃ absorption is already taken into account in the line calculations, and MODIS band-averaged O₃ absorption is smaller than the absorption at the central wavelength, which was set to $\lambda_c = 640$ nm with reference to SEVIRI. In general, atmospheric correction factors are modest in this wavelength band, with the largest effect caused by water vapour, a somewhat smaller effect by O₃ and a marginal contribution by O₂.

Figure 3 illustrates the dependence of the atmospheric correction on AMF, CTH and TCWV. Obvious features are an increase of the correction factor with AMF (longer light path), a decrease with CTH (shorter light path), and an increase with TCWV. At large CTH, ozone remains as the only significant absorber, with a slightly negative correction factor for MODIS as was noted before. In general, the differences between the satellite instruments are relatively small.

3.2 0.8 μ m

The three satellite instruments have very different SRFs for the 0.8- μ m channel. The MODIS and SEVIRI bands are both relatively narrow, with the former shifted to larger wavelengths. In contrast, the AVHRR channel is very broad, about 300 nm. Absorption is due to water vapour, while the O₂-A band yields additional absorption in the AVHRR channel only. The MODIS channel is located such that water vapour has a minimal influence. SEVIRI suffers much more from absorption by water vapour, and for AVHRR the effect is largest, more than 10%.

3.3 1.6 μ m

In the 1.6- μ m channel again MODIS has the narrowest band. The AVHRR band is broader and shifted towards lower wavelengths. The SEVIRI band is centered around the same wavelength as MODIS but is about 4 times as broad. As a result, the instruments have different sensitivities to trace gas absorption. MODIS is equally

Table 2: Satellite instrument channels considered in this study. Both the ‘approximate’ wavelengths, used throughout this report to indicate the channels, and the wavelengths used for the monochromatic DAK calculations are given.

wavelength (μm)		channel number		
approximate	DAK λ_c	SEVIRI	MODIS	AVHRR
0.6	0.64	1	1	1
0.8	0.82	2	2	2
1.6	1.63	3	6	3a
2.1	2.11	-	7	-
3.8	3.83	4	20	3b

Table 3: Atmospheric correction factors for a reference atmosphere (CTH = 2 km, AMF = 2, and TCWV = 30 kg m⁻²). Correction factors are given as $(1 - c) \times 100\%$, for individual absorbing gases and for all gases together. S, M and A refer to SEVIRI, MODIS and AVHRR, respectively. If absorption by a gas has no or less than 0.01% effect on c , this is indicated by a ‘-’. The totals for all gases may differ somewhat from the sum of the individual gases because of rounding effects, interaction with Rayleigh scattering, and saturation effects. For the 3.8- μm channel, the absorption of individual gases are presented additive to the N₂-continuum (since N₂ could not be switched off in MODTRAN). This explains why CO₂ has a relatively low impact for SEVIRI, even though it absorbs all radiation between 4.2 and 4.45 μm .

gas	0.6 μm			0.8 μm			1.6 μm			2.1 μm	3.8 μm		
	S	M	A	S	M	A	S	M	A	M	S	M	A
H ₂ O	0.5	0.8	0.6	5.7	1.1	10.6	0.6	0.2	0.2	3.1	6.0	9.6	11.9
CO ₂	-	-	-	-	-	-	1.9	0.9	3.1	2.9	4.6	0.3	0.2
CH ₄	-	-	-	-	-	-	0.8	0.8	0.1	0.04	1.5	1.8	3.7
N ₂ O	-	-	-	-	-	-	-	-	-	0.3	3.4	2.5	1.6
O ₃	0.3	-0.4	0.7	-	-	-	-	-	-	-	-	-	-
O ₂	0.2	0.2	0.1	0.04	-	1.7	-	-	-	-	-	-	-
N ₂	-	-	-	-	-	-	-	-	-	-	10.3	1.0	0.7
All gases	1.0	0.6	1.5	5.7	1.1	12.3	3.4	1.9	3.4	6.3	25.5	14.9	17.6

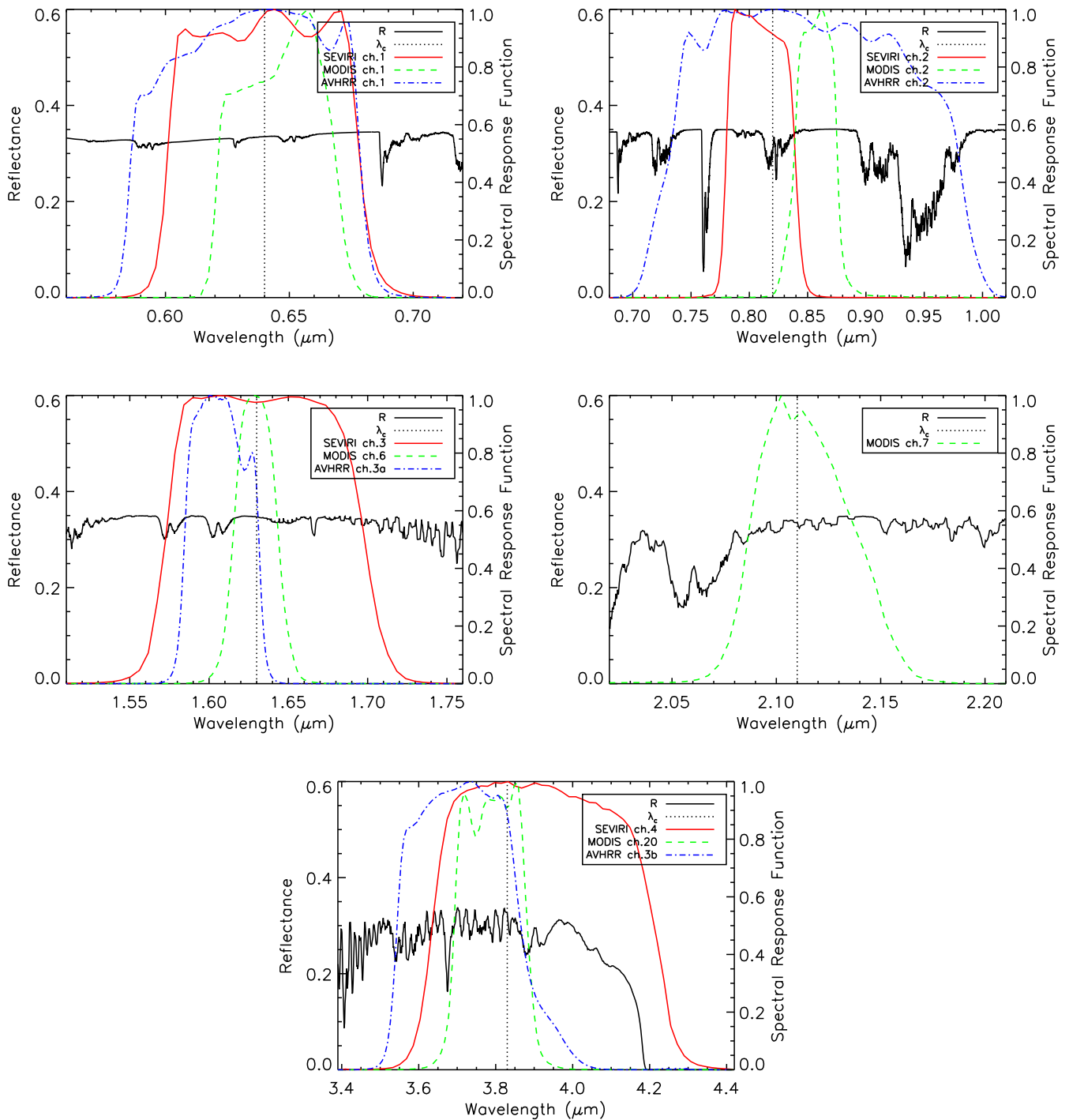


Figure 2: Reflectance spectra (solid black) and spectral response functions of SEVIRI (solid red), MODIS (dashed green), and AVHRR (dash-dotted blue) for the 0.6-, 0.8-, 1.6-, 2.1-, and 3.8- μm channels. More details on the SRF data are provided in Appendix B. The dotted lines represent the central wavelengths λ_c used for creating the CPP LUT with DAK. The reflectance spectra were generated for a reference atmosphere (CTH = 2 km, AMF = 2, and TCWV = 30 kg m^{-2}).

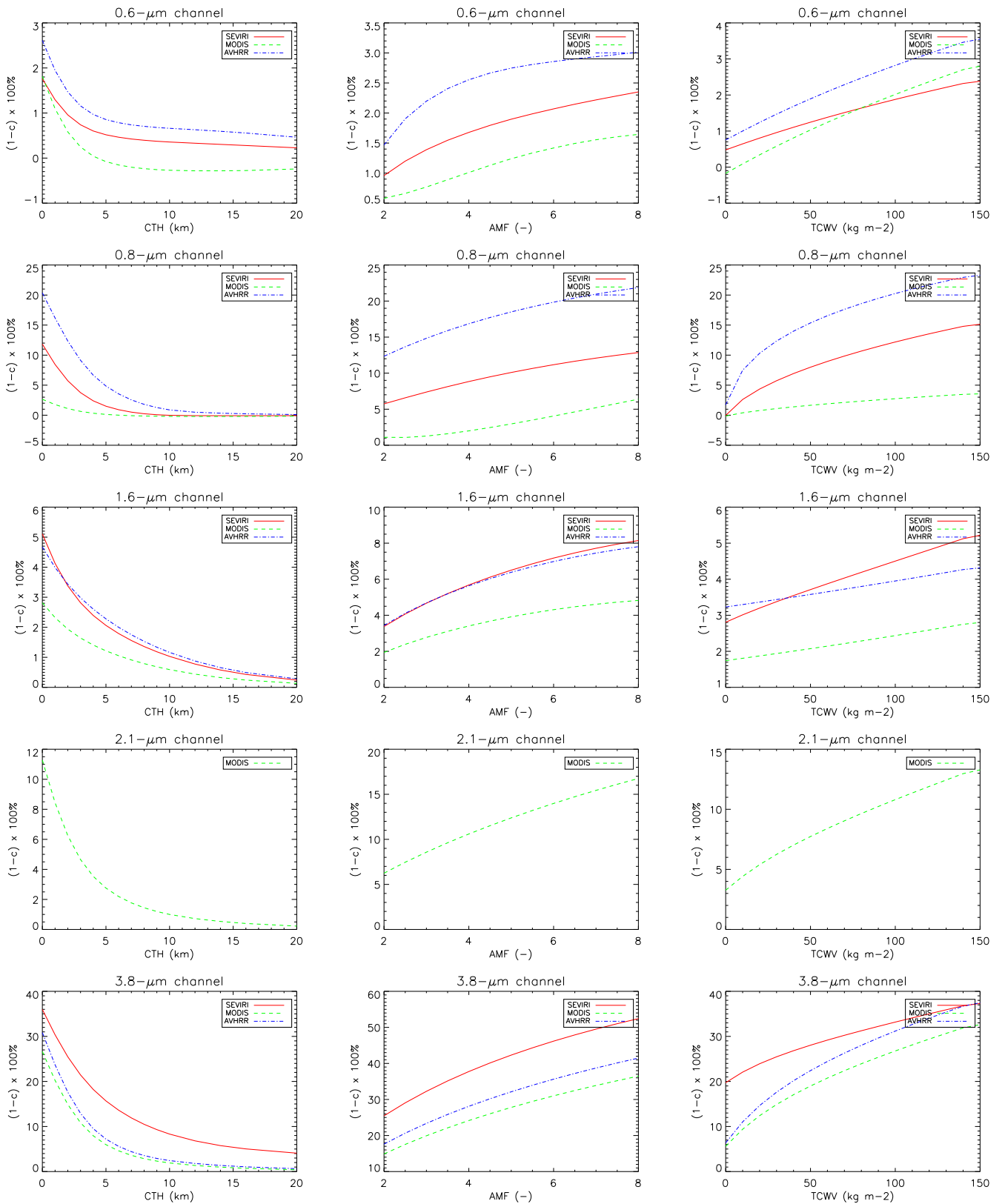


Figure 3: Atmospheric correction factors as a function of AMF, CTH and TCW. In each plot, one of these parameters is varied, while the others are kept at their value in the reference atmosphere (CTH = 2 km, AMF = 2, and TCW = 30 kg m^{-2}).

affected by CO_2 and CH_4 , SEVIRI is more affected by CO_2 (and somewhat by water vapour), and for AVHRR CO_2 is the only trace gas with considerable absorption.

3.4 2.1 μm

The 2.1- μm channel is only available on MODIS. Absorption by water vapour and CO_2 have a considerable impact on the reflectances, while minor contributions are due to N_2O and CH_4 .

3.5 3.8 μm

For the 3.8- μm channel, the MODIS and AVHRR bands are relatively similar, but the SEVIRI band is much broader, extending to larger wavelengths. For this reason, SEVIRI is affected by N_2 -continuum absorption, taking place between about 3.9 and 4.6 μm , while this has hardly any effect on the other instruments. Similarly, SEVIRI is the only instrument seriously influenced by the strong CO_2 absorption starting around 4.1 μm . All instruments are affected significantly by water vapour, N_2O and CH_4 absorption. Altogether, the atmospheric correction for the 3.8- μm channels is much larger than for any other channel.

4 Impact on CPP retrievals

The atmospheric correction scheme has been implemented in CPP version 3.0. The previous CPP version (2.3) already contained an atmospheric correction procedure based on SCIAMACHY spectra (Roebeling et al. 2006). The corresponding correction factors were small and only dependent on the viewing zenith angle ($0.0\% < 1 - c < 0.7\%$ at 0.6 μm and $1.0\% < 1 - c < 2.5\%$ at 1.6- μm for $0^\circ < \theta < 75^\circ$). In this section, the impact of the new atmospheric correction method on CPP retrievals is assessed, not in comparison to the old method but in comparison to neglecting atmospheric correction.

We focus on retrievals from SEVIRI over Europe using the standard CPP algorithm, i.e. based on the 0.6- and 1.6- μm channels. Winter (January) and summer (July) retrievals at three times during the day (8:00, 12:00 and 16:00 UTC) have been considered, to obtain a large spread in solar zenith angle (and thus AMF). From both months three days (5, 15, and 25 Jan./Jul.) have been selected, to keep the data volume within acceptable limits. Hence, a total of 18 SEVIRI images have been analysed.

Figure 4 shows histograms of the atmospheric correction factors and their impact on retrieved cloud physical parameters. To first order, the 0.6- μm reflectance depends on the cloud optical thickness (COT or τ). Atmospheric correction leads to a reduction in the reflectances as tabulated in the CPP LUT. Hence, a given reflectance measurement corresponds to a larger τ when atmospheric correction is applied. The 1.6- μm reflectance determines the cloud droplet effective radius (r_e), but since these variables have an inverse relationship (smaller droplets reflect more), atmospheric correction leads to a reduction in r_e . The relative reduction in r_e is larger than the relative increase in τ , which is partly related to the much larger impact of trace-gas absorption in the 1.6- μm channel compared to the 0.6- μm channel. Cloud water path (CWP) is proportional to the product of τ and r_e . Therefore, it generally experiences a reduction due to atmospheric correction.

The results in Figure 4 are not completely straightforward to explain. For example, a non-negligible fraction of pixels shows a decrease (increase) in τ (r_e). This is partly explained by retrieval of a different thermodynamic phase for some pixels (i.e. ice phase without and water phase with atmospheric correction), but is also related to peculiar shapes of the $R_{0.6}$ - $R_{1.6}$ diagram for specific viewing geometries, and particularly for lower optical thicknesses.

In Figure 5 the impact of atmospheric correction on τ and r_e ($\Delta\tau$ and Δr_e , respectively) is stratified with respect to two parameters governing the atmospheric correction: AMF and CTH. As expected, $\Delta\tau$ increases with increasing AMF. For Δr_e the expected relation is also present, but less clear. With increasing CTH, one

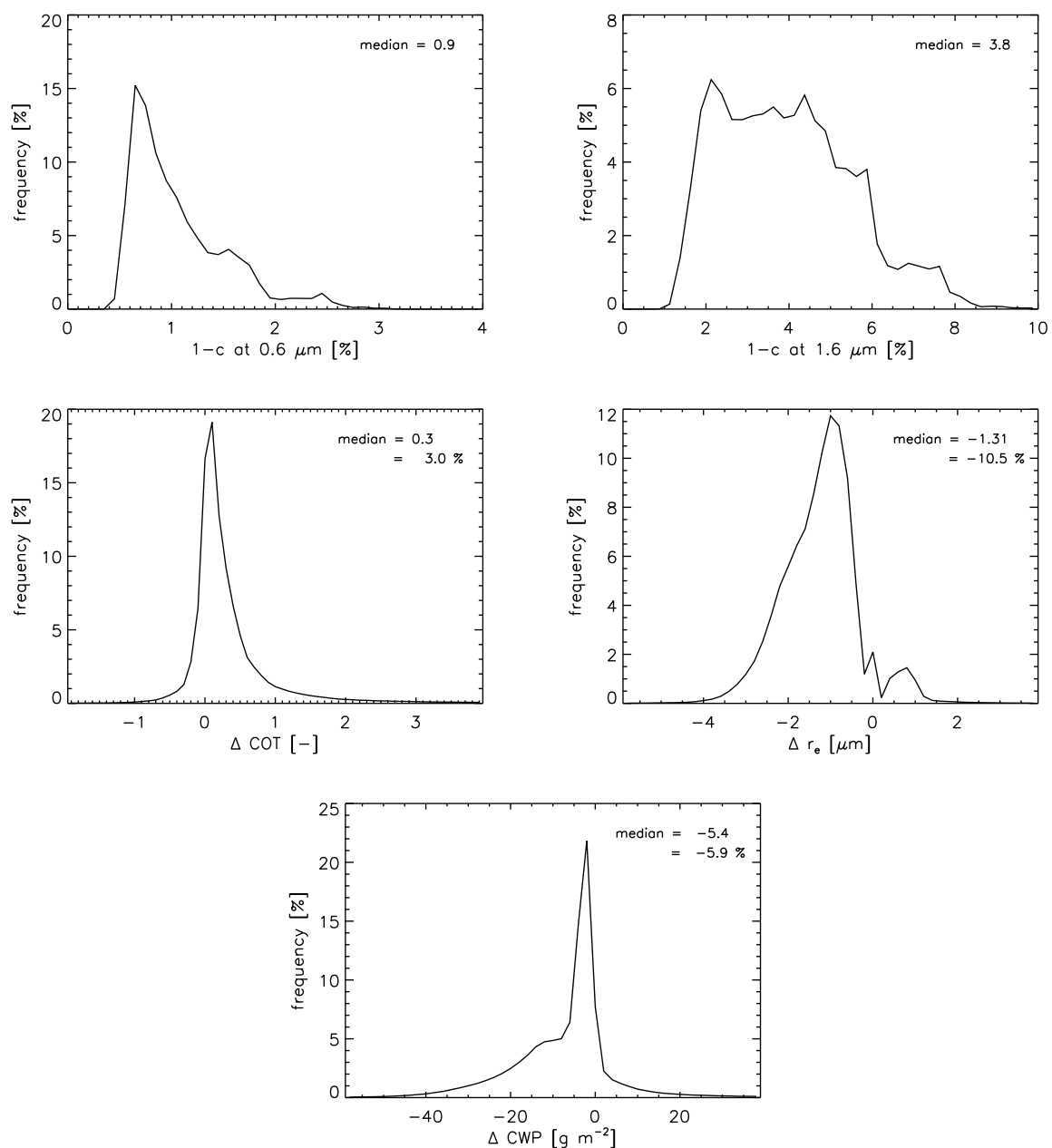


Figure 4: Histograms of atmospheric correction factors $1 - c$ (for 0.6- and 1.6- μm channels) and differences Δ between retrieved cloud physical properties, τ ($= \text{COT}$), r_e , and CWP, with and without atmospheric correction, i.e. $\Delta\tau = \tau_{\text{with atmospheric correction}} - \tau_{\text{without atmospheric correction}}$, etc. The median of the differences is also indicated, both as absolute number and as a percentage of the median without atmospheric correction. The plots are based on 18 SEVIRI images over Europe, as described in the text. Only pixels with $\tau > 4$ (with and without atmospheric correction) were considered, leading to 1,294,804 selected pixels.

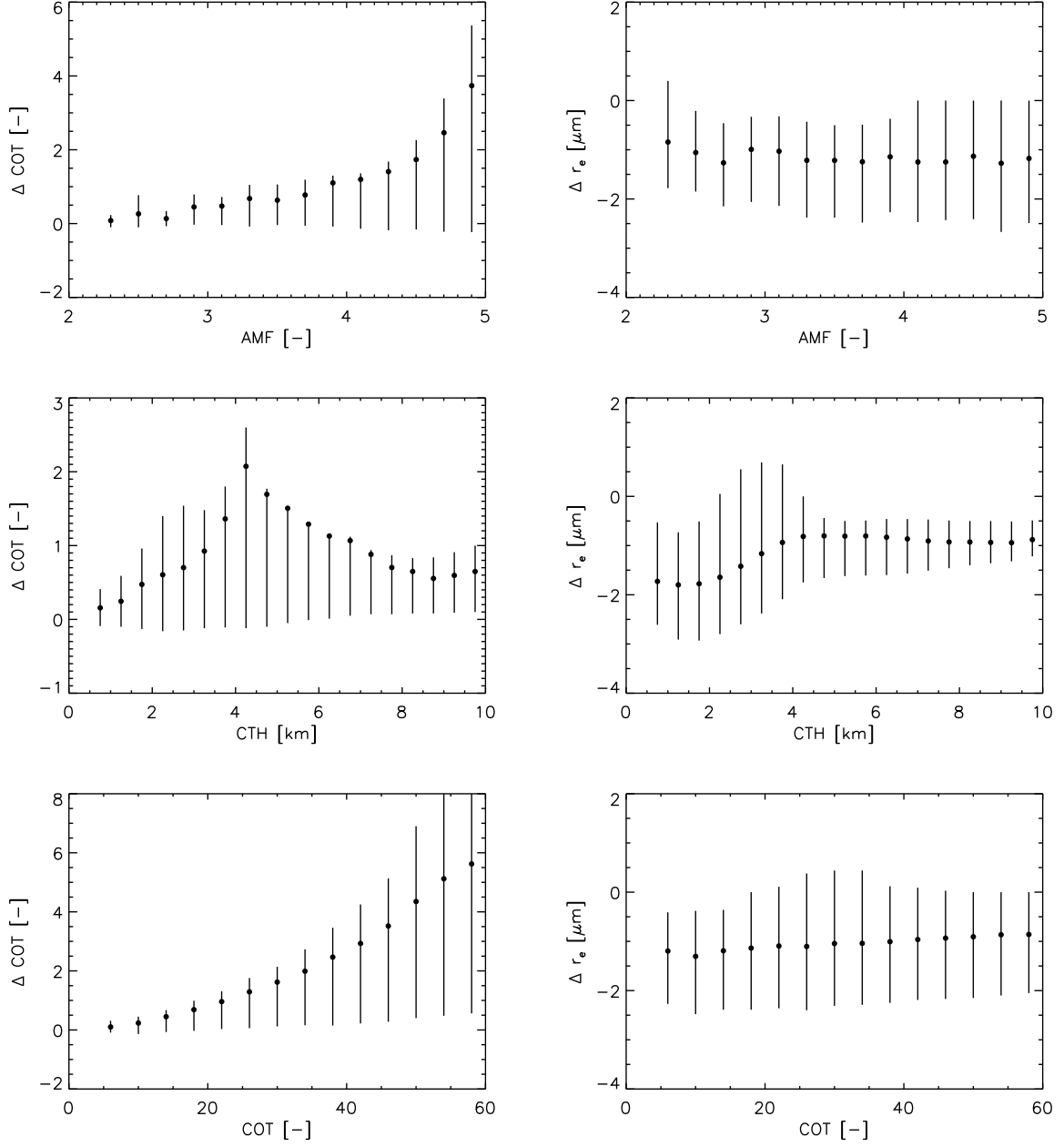


Figure 5: Differences Δ between retrieved cloud physical properties, τ ($= \text{COT}$) and r_e , with and without atmospheric correction as a function of AMF, CTH, and COT. The data are the same as in Figure 4. The symbols denote the mean ΔCOT (Δr_e) in the respective AMF (CTH, COT) bin, while the vertical bars denote the 0.1–0.9 percentile range.

would expect $\Delta\tau$ to decrease. This is indeed true for CTH larger than 4 km, but not for lower values. The reason becomes apparent when $\Delta\tau$ is plotted as a function of τ . Due to the logarithmic-like dependence of the 0.6- μm reflectance on τ , a change in reflectance has a stronger effect at larger τ . Therefore, the (absolute) effect of atmospheric correction increases when τ increases. Since CTH is positively correlated with τ , an increase in CTH then leads to an increase in $\Delta\tau$. At larger CTH, the contribution of – high but relatively thin – cirrus clouds plays a role, and the expected decrease of $\Delta\tau$ with CTH is found. Finally, the dependence of Δr_e on CTH is qualitatively as expected. Stratifications with respect to TCWV are not shown, since TCWV experiences little spatio-temporal variation in our dataset, except for a factor ≈ 2 difference between summer and winter (see Figure 1).

In other regions than Europe, atmospheric corrections will have different impacts on retrieved cloud physical properties. For example, over tropical Africa effects are expected to be larger because of larger water vapour columns, but smaller because of smaller satellite viewing zenith angles. For polar-orbiting instruments, like AVHRR and MODIS, effects will be different because of different SRFs, as presented Section 3.

5 Future work and improvements

The atmospheric correction scheme developed in this study can be improved in a number of ways:

- Instead of using climatological TCWV from ISCCP combined with fixed vertical water vapour profiles, it would be better to take actual modelled water vapour profiles from which the partial column above the cloud could be determined and fed into the atmospheric correction procedure. In this way, the strong spatio-temporal variability of water vapour would be taken into account much better.
- Alternative retrievals of cloud top height are available from the CM-SAF processing chain. These more advanced algorithms may give an improved CTH estimate.
- A more precise correction for Rayleigh scattering could be added. The DAK calculations include Rayleigh scattering, but only for a standard cloud altitude between 1 and 2 km. The contribution of Rayleigh scattering to the reflectance is different for higher/lower clouds, which is currently not taken into account.
- A final issue is absorption by trace gases below and inside the cloud. Since the part of the total reflectance coming from below the cloud is calculated within CPP, the additional below-cloud absorption can in principle be estimated in the same way as above-cloud absorption. However, it was decided not to implement this at the moment, because there is only a significant impact for thin clouds, which anyway have a large uncertainty in their retrieved physical parameters. Trace-gas absorption within the cloud could be estimated from MODTRAN simulations including clouds (as opposed to representing clouds with a Lambertian surface). However, Roebeling et al. (2005) indicated that there are some issues with the representation of clouds in MODTRAN. For this reason, and also because the effect is probably small and the uncertainties associated with trace-gas profiles are relatively large, it was decided to ignore in-cloud absorption at the moment.

A consequence of the implementation of atmospheric correction is that re-calibration coefficients have to be updated. For example, for the SEVIRI retrievals shown in Section 4, re-calibration (with respect to the calibration at EUMETSAT) coefficients of 1.04 and 1.03 were applied to the measured 0.6- and 1.6- μm reflectances, respectively. These coefficients were derived from a comparison with MODIS, not taking into account differences in SRFs, and have to be updated when atmospheric correction is introduced in CPP.

6 Summary

An atmospheric correction method based on MODTRAN4.2 radiative transfer simulations has been implemented in the CPP retrieval algorithm (version 3.0). This method accounts for the effect of absorption by atmospheric gases (H_2O , CO_2 , CH_4 , N_2O , O_3 , O_2 , and N_2) on spectral-band-averaged TOA reflectances as observed by satellite instruments. Correction factors have been calculated for three instruments (SEVIRI, MODIS, and AVHRR) and five spectral bands (around wavelengths 0.6, 0.8, 1.6, 2.1, and $3.8 \mu\text{m}$). CPP retrievals over Europe based on the 0.6- and $1.6\text{-}\mu\text{m}$ channels from SEVIRI have been analysed, indicating a $\sim 3\%$ increase in τ and a $\sim 10\%$ decrease in r_e as a consequence of atmospheric correction.

A MODTRAN input file

Here is an example of a MODTRAN 4.2 input file for a simulation of the reflectance in the $0.6\text{-}\mu\text{m}$ channel for $\text{CTH} = 5 \text{ km}$, $\text{AMF} = 3.5$ ($\theta_0 = \theta = 55.15^\circ$), and $\text{TCWV} = 40 \text{ kg m}^{-2}$.

```

M 7 2 2 1 2 2 2 2 2 2 1 1 0 273.000 0.350
f 0f 0 385.000 + 1.370 1.000
0 0 0 0 0 0 .000 .000 .000 .000 .000
31 1 0
5.000 A A
3.200e-01 1.700e+00
6.000 A A
3.200e-01 1.700e+00
:
25.000 A A
3.200e-01 1.700e+00
30.000 A A
3.200e-01 1.700e+00
:
60.000 A A
3.200e-01 1.700e+00
70.000 A A
3.200e-01 1.700e+00
80.000 A A
3.200e-01 1.700e+00
100.000 A A
3.200e-01 1.700e+00
100.000 5.000 124.850 0.000 0.000 0.000 0 0.000
2 2 93 0
0.000 55.150 0.000 0.000 0.000 0.000 0.000 0.000
560 720 1 1rn nlaa
0

```

B Spectral Response Functions

SEVIRI SRFs were downloaded from http://www.eumetsat.int/Home/Main/What_We_Do/Satellites/Meteosat_Second_Generation/Space_Segment/SP_1138096039033?l=en. SRFs are reported for the SEVIRI instruments on MSG-1, MSG-2, and MSG-3. We have used the MSG-1 SRFs in this study, but verified that differences

with the other instruments are negligible for our purpose. For the 3.8- μm channel, SRFs are reported at two temperatures: 85 K and 95 K. We have used the 85-K data, but differences are again negligible.

MODIS SRFs were downloaded at ftp.mcst.ssai.biz from /pub/permanent/MCST/PFM.L1B.LUT.4-30-99/Reference_RSR_Dataset. These data are for Terra (PFM instrument). Differences with Aqua (FM1) were not checked. In MODIS terminology, spectral regions are called bands, and for each band a number of different channels are present on the instrument (bands 1 and 2 have 40 channels, corresponding to a horizontal resolution of 250 m; bands 3 to 7 have 20 channels and 500 m resolution; bands 8 to 36 have 10 channels and 1000 m resolution). We took for every band the SRF of the first channel, but noticed that SRFs for different channels are nearly identical.

AVHRR SRFs were downloaded from <http://www2.ncdc.noaa.gov/docs/klm/html/d/app-d1.htm>. These are the SRFs of AVHRR/3 on NOAA-15. The SRFs of AVHRR/3 on NOAA-13, -15, -16, -17, and -18 are similar, although differences are in some cases non-negligible (e.g., between channels 3a from NOAA-15 and NOAA-18). The earlier versions of the AVHRR instrument (AVHRR/1 onboard NOAA-6, -8, and -10; AVHRR/2 onboard NOAA-7, -9, -11, -12, and -14) did not have the 1.6- μm channel. Also, the SRFs appear to be somewhat different, in particular for the 0.8- μm channel.

C List of acronyms

Acronym	Definition
AMF	Air-Mass Factor
AVHRR	Advanced Very High Resolution Radiometer
CM-SAF	Satellite Application Facility on Climate Monitoring
COT	Cloud Optical Thickness
CPP	Cloud Physical Properties
CTH	Cloud Top Height
CWP	Cloud Water Path
DAK	Doubling Adding KNMI
EOS	Earth Observation System
EUMETSAT	European Organization for the Exploitation of Meteorological Satellites
ISCCP	International Satellite Cloud Climatology Project
KNMI	Royal Netherlands Meteorological Institute
LUT	Lookup Table
METOP	Meteorological Operational Satellite
MLS	Mid-Latitude Summer
MODIS	Moderate Resolution Imaging Spectroradiometer
MODTRAN	Moderate Resolution Atmospheric Transmission
MSG	Meteosat Second Generation
NOAA	National Oceanic and Atmospheric Administration
RTM	Radiative Transfer Model
SCIAMACHY	Scanning Imaging Absorption Spectrometer for Atmospheric Chartography
SEVIRI	Spinning Enhanced Visible and Infrared Imager
SRF	Spectral Response Function
TCWV	Total Column Water Vapour
TOA	Top Of Atmosphere

References

- Berk, A., G. P. Anderson, P. K. Acharya, J. H. Chetwynd, L.S. Bernstein, E. P. Shettle, M. W. Matthew, and S. M. Adler-Golden, 2000: MODTRAN4 Version 2 Users Manual. Technical report, Air Force Materiel Command, Air Force Research Laboratory, Space Vehicles Directorate, Hanscom AFB, MA 01731, USA.
- Berk, A., L. s. Bernstein, and D. C. Robertson, 1989: MODTRAN: A moderate resolution model for LOW-TRAN 7. Technical Report GL-TR-89-0122, Geophysics Directorate, Phillips Laboratory, Hanscom AFB, MA 01731, USA.
- Liou, K. N., 2002: *An introduction to atmospheric radiation, Second edition*. Academic Press.
- Nakajima, T. and M. King, 1990: Determination of the optical thickness and effective particle radius of clouds from reflected solar radiation measurements. Part I: Theory. *J. Atmos. Sci.*, **47**, 1878–1893.
- Podlasly, C., 2002: Correction of the surface reflectance with BRDF to improve cloud detection. Visiting Scientist Report within the SAF on Climate Monitoring of EUMETSAT, Deutscher Wetterdienst, Remote Sensing Division, Offenbach, Germany.
- Roebeling, R. A., A. Berk, A. J. Feijt, W. Frerichs, D. Jolivet, A. Macke, and P. Stammes, 2005: Sensitivity of cloud property retrievals to differences in narrow band radiative transfer simulations. Technical Report WR-2005-02, Royal Netherlands Meteorological Institute (KNMI), De Bilt, The Netherlands.
- Roebeling, R. A., A. J. Feijt, and P. Stammes, 2006: Cloud property retrievals for climate monitoring: implications of differences between SEVIRI on METEOSAT-8 and AVHRR on NOAA-17. *J. Geophys. Res.*, **111**, D20210. doi:10.1029/2005JD006990.
- Roebeling, R. A. and I. Holleman, 2008. Validation of rain rate retrievals from SEVIRI using weather radar observations. EUMETSAT Meteorological Satellite Conference, 8-11 September 2008, Darmstadt, Germany.
- Schulz, J., P. Albert, H. D. Behr, D. Caprion, H. Deneke, S. Dewitte, B. Drr, P. Fuchs, A. Gratzki, P. Hechler, R. Hollmann, S. Johnston, K.-G. Karlsson, T. Manninen, R. Miller, M. Reuter, A. Riibel, R. Roebeling, N. Selbach, A. Tetzlaff, W. Thomas, M. Werscheck, E. Wolters, and A. Zelenka, 2008: Operational climate monitoring from space: the EUMETSAT Satellite Application Facility on Climate Monitoring (CM-SAF). *Atmos. Chem. Phys. Discuss.*, **8(3)**, 8517–8563.
- Stammes, P., 2001: Spectral radiance modelling in the UV-Visible range. In Smith, W. L. and Y. M. Timofeyev, editors, *IRS 2000: Current problems in Atmospheric Radiation*, pages 385–388. A. Deepak, Hampton, VA.
- Vermote, E. F., N. El Saleous, C. O. Justice, Y. J. Kaufman, J. L. Privette, L. Remer, J. C. Roger, and D. Tanré, 1997: Atmospheric correction of visible to middle-infrared EOS-MODIS data over land surfaces: Background, operational algorithm and validation. *J. Geophys. Res.*, **102(D14)**, 17,131–17,141.

